Meccanica (2017) 52:2069–2080
DOI 10.1007/s11012-016-0569-x

Mathematical model for cold rolling based on energy method

Y. M. Liu · J. Sun · Q. L. Wang · D. H. Zhang · D. W. Zhao

Received: 5 March 2016 / Accepted: 21 October 2016 / Published online: 8 November 2016

Abstract There is an increasing requirement for improved accuracy of the rolling models which are widely used in rolling plant in order to produce high-quality products, because this accuracy is important for rolling schedule setup and automatic control. A three-dimensional mathematical model for cold rolling using tangential velocity field and energy method is firstly proposed to investigate the deformation of the strip at the roll gap based on elastic and plastic mechanics. The field and geometrical approximation yield criterion are used to integrate the internal plastic deformation power. The friction power is analyzed using the co-line vector inner product method. Finally, the analytical expressions of roll separating force and roll torque are obtained quickly considering the effect of roll flattening on the roll separating force. The predicted roll separating forces are consistent with other researchers' models, especially for on-line measured roll separating forces in a tandem cold rolling plant. The accurate predicted results provide valuable guidelines for optimization of rolling process.

Y. M. Liu · J. Sun (✉) · Q. L. Wang · D. H. Zhang · D. W. Zhao
State Key Laboratory of Rolling and Automation, Northeastern University, Shenyang 110819, Liaoning, People's Republic of China
e-mail: liuymhpj@yeah.net

Keywords Cold rolling · Tangential velocity field · Energy method · Flattened roll · Roll separating force

List of symbols

$h_{\text{in}}, h_{\text{out}}$	Half of the initial and final strip thickness at entry and exit respectively
h_0, h_1	Half of the initial and final strip thickness at entry and exit in plastic deformation zone
h_{mb}, h_{mf}	Half of the average strip thickness in backward and forward slip zone respectively
$\Delta h_{\text{in}}, \Delta h_{\text{out}}$	Half of the reduction in elastic deformation and recovery zones respectively
h_x (h_α)	Half of the strip thickness
E_s, E_r	Young's modulus of strip and roll
ν_s, ν_r	Poisson ratio of strip and roll
$\sigma_{\text{sin}}, \sigma_{\text{sout}}$	Resistance of strip deformation at entry and exit sides
σ_b, σ_f	Backward and forward tension stresses
Δh	Half of the reduction in plastic zone $\Delta h = h_0 - h_1$
R	Original radius of work roll
R_0	Flattened roll radius of work roll
l	Projected length of roll-strip contact arc in plastic deformation zone
b	Strip width
θ	Bite angle
α	Contact angle

α_n	Neutral angle
U	Flow volume per second
m	Friction factor
$D(\dot{\varepsilon}_{ij})$	The power per unit volume
v_R	Roll speed
ε	Reduction ratio, $\varepsilon = \Delta h/h_0$
$\dot{W}_i$	Internal plastic deformation power
$\dot{W}_f$	Friction power
$\dot{W}_s$	Shear power
$\dot{W}_T$	Tension power
Φ	Total power
$M^p_{\min}$	Minimum value of roll torque in plastic zone
$F^p_{\min}$	Minimum value of roll separating force in plastic zone
χ	Arm factor
F^e_{in}	Roll separating force of elastic deformation zone
F^e_{out}	Roll separating force of elastic recovery zone
F	Total roll separating force
σ_s	Resistance of strip deformation considering tension stress in plastic deformation zone
M	Total roll torque
k	Yield shear stress, $k = \sigma_s/\sqrt{3}$
H_0	Initial strip thickness
n_σ	Stress effective factor

1 Introduction

Setup draft schedule is one of the most important bases for rolling schedule optimization. This requirement is directly related to accurate prediction of the roll separating force which is significant for the admissible limits of mill capabilities and thickness accuracy, especially for cold strip rolling. So, it is necessary to establish a high accuracy method to predict roll separating force.

Many studies have been reported in literature aimed at developing analytical models to predict the roll separating force and torque in cold strip rolling. The pressure distribution model along the arc of contact at the work roll and strip interface was developed by Karman using a differential equation. And then some simplified assumptions were used to solve complex differential equations. Tselikov [1] proposed some assumptions including the substitution of the contact arc by its chord, and Coulomb's model of friction, and then found a solution of Karman's differential equation considering the backward and forward strip tension stresses. Taking into account the elastic deformation of contact arcs at entry and exit, Bland and Ford [2] obtained the analytical expressions of pressure distribution and roll separating force using some predigested assumptions, thus avoiding most of the numerical integration in Orowan's [3] theory. Hill [4] developed a general relation between the roll separating force, the strip tension stress and the energy required for the deformation based on Bland–Ford's study. The method developed by Stone [5] to predict roll separating force was based on simplified slab analysis of deformation considering the effects of strip tension and flattened roll. The simplified solution for roll separating force was researched by Freshwater [6, 7] by means of eliminating the yield stress derivative term. A new dynamic model of the rolling process was established by Hu and Ehmann [8, 9] which took into consideration the influence of roll horizontal and vertical movements. Le and Sutcliffe [10] developed a new analysis for cold rolling of thin strip, and the effect of tensions on the non-dimensional load and forward slip was investigated. An online roll separating force model for cold rolling mill by numerical integration method was developed by Chen et al. [11] according to the load equilibrium equation and the boundary condition. A non-circular contact arc was obtained naturally as a part of the solution of the governing equation by Guo [12, 13] who proposed a semi-analytical solution of Karman's rolling equation. The above analytical models (also known as conventional mathematical models) were established using slab method and most of them were based on Karman's and Orowan's models. The slab method needed some assumed conditions and reduced prediction accuracy of the models. The energy method is a powerful approximate technique available to analyse metal forming processes [14]. There are relatively few studies about cold rolling using the energy method. Sezek et al. [15] analyzed cold rolling using the dual-stream function velocity field according to the energy method, but the explicit mathematical expression of rolling force was not obtained.

In recent years, finite element method has been widely used to investigate the cold rolling, which is

more intuitive and precise with the fast development of computer technology. A rigid-plastic finite-element and an elastic–plastic finite-element solution of the flat rolling process were obtained by Malinowski et al. [16] to research deformation, temperature-fields, roll separating force and roll torque. A 3D thermo-elastic plastic finite-element model coupled with a 3D heat-transfer finite-difference model was developed by Lin and Lin [17] to analyze the variation of the cold rolling characteristics of roll separating force, stress and temperature. A set-up model for tandem cold rolling mill to maximize the throughput was developed by Reddy [18]. In the Reddy's work, power consumed was calculated and compared for various reduction schedules obtained by distributing the strip thicknesses in arithmetic, geometric, harmonic and quadratic series. A 3D-rigid plastic finite element method was considered by Jiang [19] for simulating a thin strip rolling. The modeling of the shape, profile and flatness for cold rolling of thin strip with friction variation was discussed. Montmitonnet [20] proposed a coupled numerical model for hot and cold rolling process and presented a reviewing of models for the mechanical study of the cold strip. Since the computation time and memory capacity required for analytical method are much smaller than those required for analysis by the finite element method, so development of an analytical method based on energy method is also desired for practical usage.

In the present paper, a successful method has been proposed to compute the analytical solution of roll separating force in cold rolling process using energy method based on a new tangential velocity field which has not been reported to be applied to rolling. The validity of the calculated results is discussed through comparing those with other researchers' models and on-line measured ones. The change rules of neutral point and stress factor are investigated respectively.

2 Roll separating force in plastic deformation zone

The deformation zone in the roll bite can be divided into three major parts: the zone of elastic deformation, the zone of plastic deformation, and the zone of elastic recovery as shown in Fig. 1. A Cartesian coordinate system is set up at the midpoint of the entry section in plastic deformation zone and the axes x, y and z represent length, width and thickness directions of the strip respectively. Due to the symmetry of deformation zone, only a quarter is considered. The half thickness, first order derivative equations of deformation zone are as follows:

$$\begin{cases} h_x = R + h_1 - \sqrt{R^2 - (l-x)^2} \\ h_\alpha = R + h_1 - R\cos\alpha \end{cases} \tag{1}$$

$$h_x' = -\frac{l-x}{\sqrt{R^2-(l-x)^2}} = -\tan\alpha \tag{2}$$

2.1 Tangential velocity field

Deformation in the width direction is negligible [15] when the shape factor of the strip satisfies that the ratio of width/thickness is greater than 10 in cold rolling. Only elongation is considered and widespread is neglected, and then the width b remains approximately a constant. A new tangential velocity field is proposed:

$$\begin{cases} v_x = v_0\left[1+\frac{1}{\lambda}\tan\left(\lambda\frac{h_0-h_x}{h_0}\right)\right] \\ v_y = v_0 h_x'\left\{\frac{1}{h_0}\sec^2\left(\lambda\frac{h_0-h_x}{h_0}\right) - \frac{1}{h_x}\left[1+\frac{1}{\lambda}\tan\left(\lambda\frac{h_0-h_x}{h_0}\right)\right]\right\}y \\ v_z = \frac{v_0 h_x'}{h_x}\left[1+\frac{1}{\lambda}\tan\left(\lambda\frac{h_0-h_x}{h_0}\right)\right]z \end{cases} \tag{3}$$

According to Cauchy Equation, the strain rate components from Eq. (3) are:

$$\begin{cases} \dot{\varepsilon}_x = -\frac{v_0}{h_0}\sec^2\left(\lambda\frac{h_0-h_x}{h_0}\right)h_x' \\ \dot{\varepsilon}_y = v_0 h_x'\left\{\frac{1}{h_0}\sec^2\left(\lambda\frac{h_0-h_x}{h_0}\right) - \frac{1}{h_x}\left[1+\frac{1}{\lambda}\tan\left(\lambda\frac{h_0-h_x}{h_0}\right)\right]\right\} \\ \dot{\varepsilon}_z = \frac{v_0}{h_x}h_x'\left[1+\frac{1}{\lambda}\tan\left(\lambda\frac{h_0-h_x}{h_0}\right)\right] \end{cases} \tag{4}$$

where λ is undetermined parameter. In Eqs. (3)–(4), the incompressibility condition is $\dot{\varepsilon}_x + \dot{\varepsilon}_y + \dot{\varepsilon}_z = 0$; the velocity boundary conditions of entry are $v_x|_{x=0} = v_0$, $v_y|_{y=0} = 0$, and $v_z|_{z=0} = 0$; the velocity boundary condition of roll-strip contact zone is $v_z|_{z=h_x} = -v_x\tan\alpha$. So they are kinematically admissible velocity and strain rate fields. The flow volume per second $U = v_0h_0b = v_nh_nb = v_R\cos\alpha_n b(R+h_1-R\cos\alpha_n) = v_1h_1b$, and then the value of λ in various production conditions can be got.

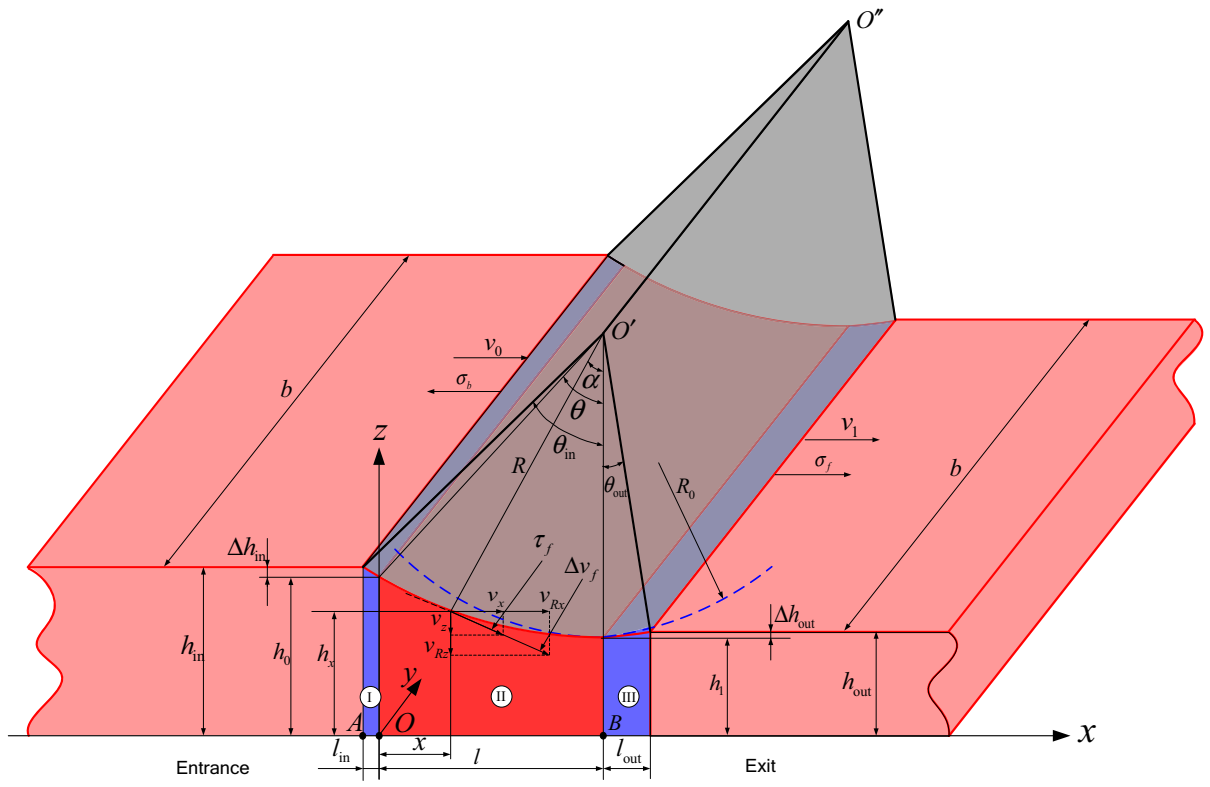

Fig. 1 Definition sketch of the roll bite zone. I, the zone of elastic deformation; II, the zone of plastic deformation; III, the zone of elastic recovery

2.2 Internal plastic deformation power

The locus of geometrical approximation (GA) yield criterion is an equilateral but non-equiangular dodecagon [21]. It lies between the loci of Tresca and TSS yield criteria and is very close to that of Mises yield criterion. GA yield criterion can well fit the classical experimental data for different ductile metals which was verified by Zhang [21]. The equations of GA yield criterion in the Haigh Westergaard stress space and the plastic power per unit volume $D(\dot{\varepsilon}_{ij})$ are ($\sigma_1 > \sigma_2 > \sigma_3$):

$$\begin{cases} \sigma_1 - \dfrac{60\sqrt{2}-16}{217}\sigma_2 - \dfrac{233-60\sqrt{2}}{217}\sigma_3 = \sigma_s, & \text{if} \quad \sigma_2 \le \dfrac{1}{2}(\sigma_1+\sigma_3) \\ \dfrac{233-60\sqrt{2}}{217}\sigma_1 + \dfrac{60\sqrt{2}-16}{217}\sigma_2 - \sigma_3 = \sigma_s, & \text{if} \quad \sigma_2 \ge \dfrac{1}{2}(\sigma_1+\sigma_3) \end{cases} \tag{5}$$

$$D(\dot{\varepsilon}_{ij}) = \frac{1000}{1683}\sigma_s(\dot{\varepsilon}_{\max} - \dot{\varepsilon}_{\min}) \tag{6}$$

Noticing $\dot{\varepsilon}_{\max} = \dot{\varepsilon}_x$, $\dot{\varepsilon}_{\min} = \dot{\varepsilon}_z$ in Eq. (4) and substituting these into the Eq. (6), GA yield criterion is adopted to integrate the internal plastic deformation power $\dot{W}_i$ as follows

$$\begin{aligned} \dot{W}_i &= \int_V D(\dot{\varepsilon}_{ij})\mathrm{d}V = \frac{4000}{1683}\sigma_s \int_0^l\int_0^b\int_0^{h_x} (\dot{\varepsilon}_{\max} - \dot{\varepsilon}_{\min})\mathrm{d}x\mathrm{d}y\mathrm{d}z \\ &= \frac{4000}{1683}\sigma_s \int_0^l\int_0^b\int_0^{h_x} \left\{ -\frac{v_0}{h_0}\sec^2\left(\lambda\frac{h_0-h_x}{h_0}\right)h_x' \right. \\ &\quad \left. -\frac{v_0}{h_x}h_x'\left[1+\frac{1}{\lambda}\tan\left(\lambda\frac{h_0-h_x}{h_0}\right)\right]\right\}\mathrm{d}x\mathrm{d}y\mathrm{d}z \\ &= \frac{4000}{1683}\sigma_s U\left[\frac{(1-\varepsilon)}{\lambda}\tan(\lambda\varepsilon) - \frac{2}{\lambda^2}\ln\cos(\lambda\varepsilon) + \varepsilon\right] \end{aligned} \tag{7}$$

2.3 Friction power

The friction only acts on the interface between the roll and strip. Note that the friction stress $\boldsymbol{\tau}_f = m\boldsymbol{k}$ and tangential velocity discontinuity $\Delta\boldsymbol{v}_f$ are always co-line vectors on the interface, as shown in Fig. 1, so the concrete co-line vector inner product [22] is used

to integrate the friction power $\dot{W}_f$. It is found ("Appendix 1")

$$\dot{W}_f = 4mkbR\left\{\frac{U}{h_0 b}\left[\left(1+\frac{g_b}{\lambda}\right)\times \ln\frac{(1+\cos\alpha_n+\sin\alpha_n)(1+\cos\theta-\sin\theta)}{(1+\cos\alpha_n-\sin\alpha_n)(1+\cos\theta+\sin\theta)} + \left(1+\frac{g_f}{\lambda}\right)\ln\frac{1+\cos\alpha_n+\sin\alpha_n}{1+\cos\alpha_n-\sin\alpha_n}\right] + v_R(\theta-2\alpha_n)\right\} \tag{8}$$

where m is friction factor calculated in Ref. [11], g_b and g_f are the parameters of backward and forward slip zone, $g_b = \tan\left(\lambda\frac{h_0-h_{mb}}{h_0}\right)$, $g_f = \tan\left(\lambda\frac{h_0-h_{mf}}{h_0}\right)$, $h_{mb} = \frac{h_0+2h_{z_n}}{3}$, $h_{mf} = \frac{h_{z_n}+2h_1}{3}$.

2.4 Shear power

According to Eqs. (1), (2) and (3), there is $h'_{x=l} = h'_{\alpha=0} = 0$, $v_z|_{x=l} = v_y|_{x=l} = 0$ in the exit section $(x = l)$ of deformation zone. Therefore, there is no shear power in the exit section. But on the entry section $(x = 0)$

$$v_y|_{x=0} = 0, v_z|_{x=0} = -\frac{v_0\tan\theta}{h_0}z \tag{9}$$

There exists discontinuous velocity. Then the shear power $\dot{W}_s$ is required for shear action along the surface of velocity discontinuity as follows

$$\begin{aligned}\dot{W}_s &= 4k\int_0^{h_0}\int_0^{b_0}|\Delta v_t|\mathrm{d}y\mathrm{d}z \\ &= 4k\int_0^{b}\int_0^{h_0}\frac{v_0\tan\theta}{h_0}z\mathrm{d}y\mathrm{d}z \\ &= 2kbh_0v_0\tan\theta \\ &= 2kU\tan\theta\end{aligned} \tag{10}$$

2.5 Tension power

Tension stress technology between stands must be used in the modern cold rolling process for reducing roll separating force and improving flatness quality. The tension power $\dot{W}_T$ is

$$\dot{W}_T = 4\left(\sigma_b bh_0v_0 - \sigma_f bh_1v_1\right) = 4U\left(\sigma_b - \sigma_f\right) \tag{11}$$

2.6 Total power functional and its minimization

Substituting Eqs. (7), (8), (10) and (11) into the total power functional $\Phi = \dot{W}_i + \dot{W}_f + \dot{W}_s + \dot{W}_T$, the analytical solution of total power functional Φ can be received

$$\begin{aligned}\Phi = {} & \frac{4000}{1683}\sigma_s U\left[\frac{(1-\varepsilon)}{\lambda}\tan(\lambda\varepsilon) - \frac{2}{\lambda^2}\ln\cos(\lambda\varepsilon) + \varepsilon\right] \\ & + 2kU\tan\theta + 4U\left(\sigma_b - \sigma_f\right) + 4mkbR \\ & \left\{v_R(\theta-2\alpha_n) + \frac{U}{h_0 b}\left[\left(1+\frac{g_b}{\lambda}\right)\right.\right. \\ & \ln\frac{(1+\cos\alpha_n+\sin\alpha_n)(1+\cos\theta-\sin\theta)}{(1+\cos\alpha_n-\sin\alpha_n)(1+\cos\theta+\sin\theta)} \\ & \left.\left.+\left(1+\frac{g_f}{\lambda}\right)\ln\frac{1+\cos\alpha_n+\sin\alpha_n}{1+\cos\alpha_n-\sin\alpha_n}\right]\right\}\end{aligned} \tag{12}$$

The total power of Eq. (12) is minimized with respect to the arbitrary variable α_n, and then the value closest to the actual power required is got. Differentiating the total power and setting it to be zero, and then the following equation can be obtained

$$\frac{\mathrm{d}\Phi}{\mathrm{d}\alpha_n} = \frac{\mathrm{d}\dot{W}_i}{\mathrm{d}\alpha_n} + \frac{\mathrm{d}\dot{W}_f}{\mathrm{d}\alpha_n} + \frac{\mathrm{d}\dot{W}_s}{\mathrm{d}\alpha_n} + \frac{\mathrm{d}\dot{W}_T}{\mathrm{d}\alpha_n} = 0 \tag{13}$$

where

$$\frac{\mathrm{d}\dot{W}_i}{\mathrm{d}\alpha_n} = \frac{4000}{1683}\sigma_s N\left[\frac{(1-\varepsilon)}{\lambda}\tan(\lambda\varepsilon) - \frac{2}{\lambda^2}\ln\cos(\lambda\varepsilon) + \varepsilon\right] \tag{14}$$

$$\begin{aligned}\frac{\mathrm{d}\dot{W}_f}{\mathrm{d}\alpha_n} = {} & 4mkbR\left\{-2v_R + \frac{N}{h_0 b}\left[\left(1+\frac{g_b}{\lambda}\right)\right.\right. \\ & \ln\frac{(1+\cos\alpha_n+\sin\alpha_n)(1+\cos\theta-\sin\theta)}{(1+\cos\alpha_n-\sin\alpha_n)(1+\cos\theta+\sin\theta)} \\ & \left.+\left(1+\frac{g_f}{\lambda}\right)\ln\frac{1+\cos\alpha_n+\sin\alpha_n}{1+\cos\alpha_n-\sin\alpha_n}\right] \\ & -\frac{UR\sin\alpha_n}{3h_0^2 b}\left[2\sec^2\left(\lambda\frac{h_0-h_{mb}}{h_0}\right)\right. \\ & \ln\frac{(1+\cos\alpha_n+\sin\alpha_n)(1+\cos\theta-\sin\theta)}{(1+\cos\alpha_n-\sin\alpha_n)(1+\cos\theta+\sin\theta)} \\ & \left.+\sec^2\left(\lambda\frac{h_0-h_{mf}}{h_0}\right)\ln\frac{1+\cos\alpha_n+\sin\alpha_n}{1+\cos\alpha_n-\sin\alpha_n}\right] \\ & \left.+\frac{U}{h_0 b\cos\alpha_n}\left(2+\frac{g_b+g_f}{\lambda}\right)\right\}\end{aligned} \tag{15}$$

$$\frac{\mathrm{d}\dot{W}_s}{\mathrm{d}\alpha_n} = 2kN\tan\theta \tag{16}$$

$$\frac{\mathrm{d}\dot{W}_T}{\mathrm{d}\alpha_n} = 4N\left(\sigma_b - \sigma_f\right) \tag{17}$$

where $N = \frac{\mathrm{d}U}{\mathrm{d}\alpha_n} = v_R bR\sin 2\alpha_n - v_R b(R+h_1)\sin\alpha_n$.

The optimal value of α_n in various production conditions can be obtained by solving Eq. (13). The minimum of total power $\Phi_{\min}$ can be attained by substituting optimal value of α_n into Eq. (12). Then, the corresponding minimum values of roll torque and roll separating force in plastic deformation zone can be determined respectively [22]:

$$M^p_{\min} = \frac{R_0\left(\dot{W}_i+\dot{W}_f+\dot{W}_s\right)}{v_R}, \quad F^p_{\min} = \frac{M^p_{\min}}{2\chi\sqrt{2R\Delta h}} \tag{18}$$

3 Roll separating force in elastic deformation zone

According to generalized Hooke's law, half of the elastic deformation and recovery zones' reduction Δh_{in} and Δh_{out} are

$$\frac{\Delta h_{\text{in}}}{h_{\text{in}}} = \frac{1-v_s^2}{E_s}\sigma_{s\text{in}} - \frac{v_s(1+v_s)}{E_s}\sigma_b \tag{19}$$

$$\frac{\Delta h_{\text{out}}}{h_{\text{out}}} = \frac{1-v_s^2}{E_s}\sigma_{s\text{out}} - \frac{v_s(1+v_s)}{E_s}\sigma_f \tag{20}$$

According to Fig. 1, the projected length of the roll-strip contact arc in elastic deformation and recovery zones are $l_{\text{in}} = \sqrt{2R(\Delta h+\Delta h_{\text{in}})} - \sqrt{2R\Delta h}$ and $l_{\text{out}} = \sqrt{2R\Delta h_{\text{out}}}$ respectively.

The roll-strip contact arc in elastic deformation zone is so small that it is simplified as a chord. And the roll separating force of elastic deformation zone F^e_{in} considering backward tension stress is [23]

$$\begin{aligned} F^e_{in} &= 2b\int_{-l_{\text{in}}}^{0}\left(\frac{E_s}{1-v^2}\frac{h_{\text{in}}-h_x}{h_{\text{in}}} + \frac{v_s}{1-v_s}\sigma_b\right)\mathrm{d}x \\ &= 2b\int_{-l_{\text{in}}}^{0}\frac{E_s}{1-v^2}\frac{h_{\text{in}}-h_x}{h_{\text{in}}}\mathrm{d}x + 2b\int_{-l_{\text{in}}}^{0}\frac{v_s}{1-v_s}\sigma_b\mathrm{d}x \\ &= bh_{\text{in}}\frac{1-v_s^2}{E_s}\sqrt{\frac{R}{2\Delta h}}\left(\sigma_{s\text{in}} - \frac{v_s}{1-v_s}\sigma_b\right)^2 \\ &\quad + 2bl_{\text{in}}\frac{v_s}{1-v_s}\sigma_b \end{aligned} \tag{21}$$

The roll-strip contact arc in elastic recovery zone is predigested as a parabola. The roll separating force of elastic recovery zone F^e_{out} considering forward tension stress is

$$\begin{aligned} F^e_{\text{out}} &= 2b\int_{l}^{l+l_{\text{out}}}\left(\frac{E_s}{1-v^2}\frac{h_{\text{out}}-h_x}{h_{\text{out}}} + \frac{v_s}{1-v_s}\sigma_f\right)\mathrm{d}x \\ &= 2b\int_{l}^{l+l_{\text{out}}}\frac{E_s}{1-v^2}\frac{h_{\text{out}}-h_x}{h_{\text{out}}}\mathrm{d}x \\ &\quad + 2b\int_{l}^{l+l_{\text{out}}}\frac{v_s}{1-v_s}\sigma_f\mathrm{d}x \\ &= \frac{4}{3}b\sqrt{2Rh_{\text{out}}\frac{1-v_s^2}{E_s}\left(\sigma_{s\text{out}} - \frac{v_s}{1-v_s}\sigma_f\right)^3} \\ &\quad + 2bl_{\text{out}}\frac{v_s}{1-v_s}\sigma_f \end{aligned} \tag{22}$$

4 Calculation and discussion

4.1 Total roll separating force and torque calculations

According to Eqs. (18), (21) and (22), the total roll separating force F acting on strip elastic and plastic deformation zones is

$$F = F^e_{in} + F^e_{\text{out}} + F^p_{\min} \tag{23}$$

The total roll torque M acting on strip elastic and plastic deformation zones is

$$\begin{aligned} M &= M^p_{\min} + 2\left[F^e_{in}\left(l+\frac{l_{\text{in}}}{2}\right) - F^e_{\text{out}}\frac{l_{\text{out}}}{2}\right] \\ &= M^p_{\min} + \left[F^e_{in}(2l+l_{\text{in}}) - F^e_{\text{out}}l_{\text{out}}\right] \end{aligned} \tag{24}$$

Strip deformation resistance increases dramatically due to strain hardening in cold rolling. So, the flattened roll radius and the length of roll-strip contact arc become larger, which affects the roll separating force significantly. Therefore, the flattened roll radius' model considering the effect of elastic deformation and tension stress is used in calculation as follows [24]

$$R = R_0\left[1 + \frac{4\left(1-v_r^2\right)}{\pi E_r b}\frac{F}{\left(\sqrt{\Delta h+\Delta h_{\text{t}}+\Delta h_{\text{out}}}+\sqrt{\Delta h_{\text{out}}}\right)^2}\right] \tag{25}$$

where $\Delta h_{\text{t}} = \frac{v_s(1+v_s)}{E_s}(\sigma_b h_{\text{in}} - \sigma_f h_{\text{out}})$.

The coupling calculation between the roll separating force and roll flatten radius can be carried out by iterative computation. The computing flow chart is shown in Fig. 2 and the process terminates when the

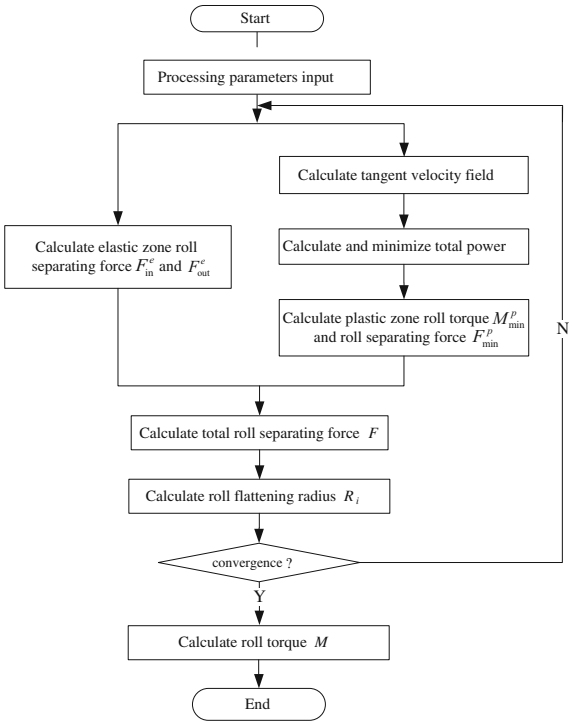

Fig. 2 Flow chart of the calculation for roll separating force

radius is convergent. The condition of convergence is $\frac{|R_i - R_{i-1}|}{R_i} \leq 0.001$ in this paper.

In order to verify the prediction capability of the analytical model in this paper, practical data of roll separating force measured in a tandem cold rolling plant are used. This production line consists of five-stand tandem cold rolling mills, and the roll separating force is measured by pressure transmitters which equipped in every stand. Taking the material of MRT-2.5 steel product for example, the strip width is 885 mm and the thickness is reduced from 2.3 to 0.28 mm in the 5 rolling stands. The roll circumferential velocity v_R and reduction ε for Nos. 1–5 stands are shown in Table 1. The regression model of deformation resistance for the MRT-2.5 steel at entry side σ_{sin}, exit side σ_{sout}, and plastic deformation zone σ_s considering tension stress can be expressed as [24] ("Appendix 2"):

$$\sigma_{sin} = \left[450.00 + \frac{264.00}{\sqrt{3}} \cdot \ln\left(\frac{H_0}{h_0}\right)\right] \times \left\{1 - 0.20\exp\left[-\frac{10.00}{\sqrt{3}} \cdot \ln\left(\frac{H_0}{h_0}\right)\right]\right\} \quad \text{(MPa)} \tag{26}$$

$$\sigma_{sout} = \left[450.00 + \frac{264.00}{\sqrt{3}} \cdot \ln\left(\frac{H_0}{h_1}\right)\right] \times \left\{1 - 0.20\exp\left[-\frac{10.00}{\sqrt{3}} \cdot \ln\left(\frac{H_0}{h_1}\right)\right]\right\} \quad \text{(MPa)} \tag{27}$$

$$\begin{aligned}\sigma_s &= \sigma - \left(0.7\sigma_b + 0.3\sigma_f\right) \times 10^{-6} \\ &= \left[450.00 + \frac{264.00}{\sqrt{3}} \cdot \ln\left(\frac{3H_0}{h_0 + 2h_1}\right)\right] \times \left\{1 - 0.20\exp\left[-\frac{10.00}{\sqrt{3}} \cdot \ln\left(\frac{3H_0}{h_0 + 2h_1}\right)\right]\right\} \\ &\quad - \left(0.7\sigma_b + 0.3\sigma_f\right) \times 10^{-6} \quad \text{(MPa)}\end{aligned} \tag{28}$$

Table 1 Rolling conditions in a plant

Stand number	1	2	3	4	5
ε (%)	33.80	37.37	37.32	31.11	32.04
σ_s (MPa)	391.29	427.03	485.97	545.47	628.48
v_R (m s^{-1})	3.95	6.34	10.20	14.75	21.85
R_0 (mm)	212.62	212.31	212.50	212.02	212.54
R (mm)	257.48	276.66	304.88	388.07	463.53
Measured roll separating force (kN)	7326.16	7605.83	6899.70	6949.97	7334.48
Measured roll torque (kNm)	75.70	61.40	42.60	25.96	20.98
Present model's roll separating force (kN)	7448.99	7785.38	7034.86	7225.51	7340.45
Present model's roll torque (kNm)	78.05	61.70	44.15	26.21	21.87
Hill model's roll separating force (kN)	7513.76	7206.62	7084.63	7236.05	7862.41
Error 1 (%)	1.68	2.36	1.96	3.96	0.08
Error 2 (%)	−0.87	7.43	−0.71	−0.15	−7.11
Error 3 (%)	3.11	0.49	3.65	0.98	4.25

Error 1: the roll separating force errors between present predictions and measured ones. Error 2: the roll separating force errors between present predictions and Hill's model. Error 3: the roll torque errors between present predictions and measured ones

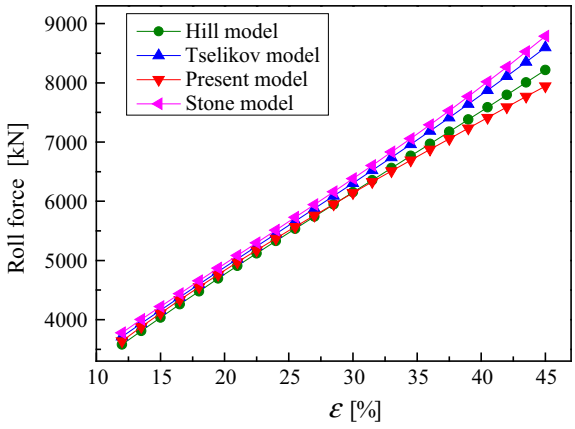

Fig. 3 Comparison roll separating force predicted by present model with other researchers' results

The roll separating force and torque determined by present model are compared to the values measured in the tandem cold rolling plant. In addition, the roll separating forces calculated by present model and Hill's model are compared, and these results are summarized in Table 1 respectively for different stands. The roll separating force and torque predicted by present model are within +3.96 and 4.25% severally of those measured in the plant. The present model's roll separating force and torque are slightly higher than the measured ones, because the upper bound method of energy method is used in this paper. The results of the present model are in a good agreement with Hill's model within ±7.43% error.

The comparison between the present model's roll separating force and the results of Hill's, Tselikov's and Stone's study under the various reductions is shown in Fig. 3. Obviously, the roll separating force increases linearly with the increasing of reduction. And this is caused by the increasing of the roll-strip contact arc and the metal plastic deformation, which leads to increase the required roll separating force. The relative percentage error among the methods is less than 10.6%, which indicates that the present approach has enough accuracy and can be applied to analyze the cold rolling process.

As shown in Fig. 2, the roll separating force is obtained by iterative computation between the roll separating force and roll flatten radius. Total iterative computation process of roll separating force and flattening radius in stand no.5 using present model [Eq. (23)] and flattened roll radius' model [Eq. (25)] is displayed in Fig. 4, and then mark every iterative step. The iteration starts with $R = R_0 = 212.54$ mm, i is iteration time, each iteration is composed of two steps: $i-1$ and $i-2$ ($i = 1, 2, \ldots 6$ in stand no. 5). $i-1$ is roll separating force calculation using Eq. (23) and roll flattening radius received in the previous step. $i-2$ is roll flattening radius calculation using Eq. (25) and roll separating force gained in the previous step. The values of roll separating force and flattening radius under iteration times in stand no. 5 are shown in Fig. 5 based on the calculation method of Fig. 4. Present model achieve the condition of convergence while iteration time is $i = 6$ according to Figs. 4 and 5. The results reflect that the roll separating force influences the roll elastic flattening obviously during cold rolling.

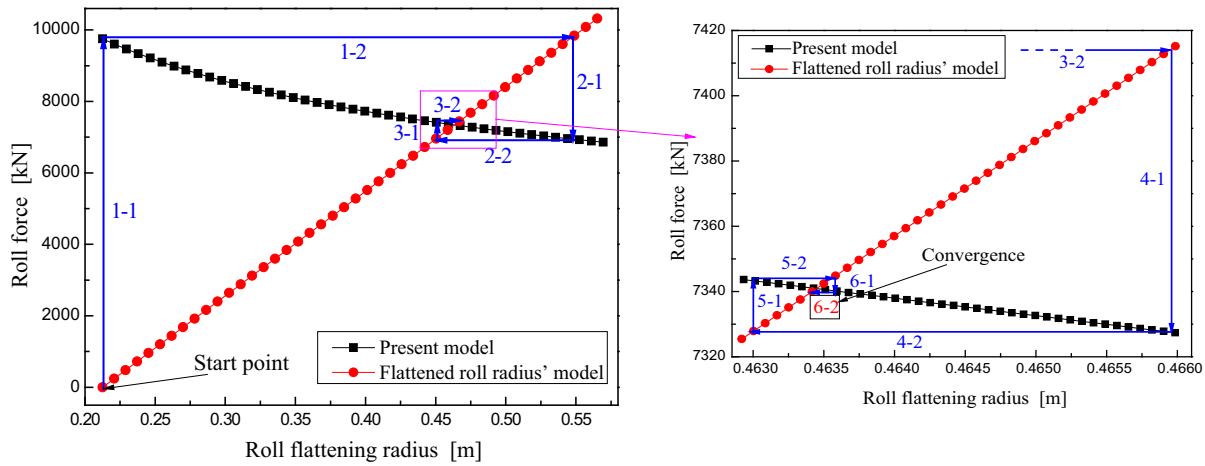

Fig. 4 Iteration process of roll separating force and flattening radius in stand no. 5

4.2 Effect of rolling parameters on location of neutral points

The value of x_n/l represents the neutral point's location. Figure 6 shows the backward and forward tension stresses are the dominant parameters of the neutral point's location. The neutral point gets close to the exit side while forward tension stress decreases or backward stress increases, because the peak value's location of compression stress between roll-strip moves toward the exit side.

It can be seen from Fig. 7 that the friction factor m and reduction ε influence the location of neutral point obviously. The forward slip decreases when m decreases or ε increases as the neutral point goes to the exit side.

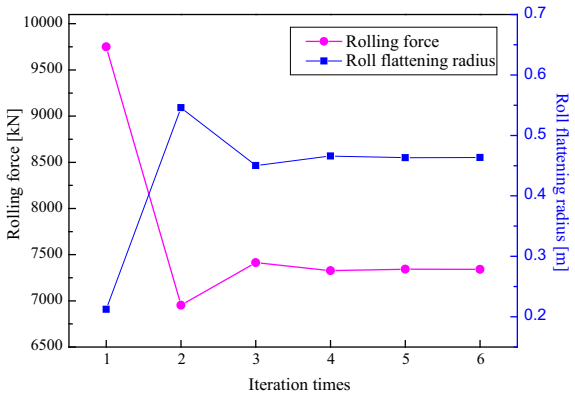

Fig. 5 Roll separating force and flattening radius under iteration times in stand no. 5

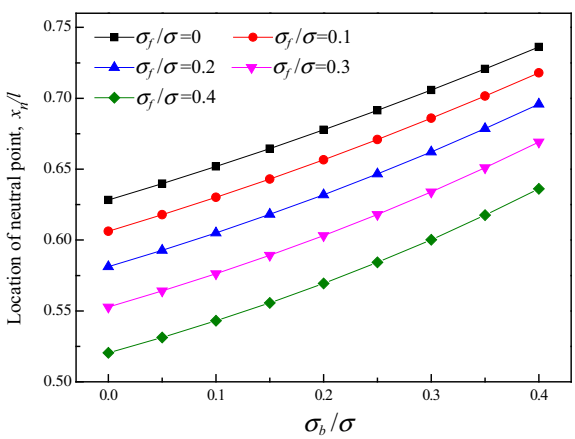

Fig. 6 Effect of tension stresses on location of neutral points

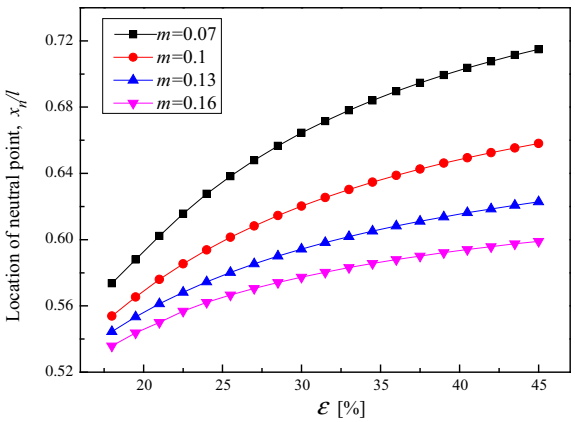

Fig. 7 Effect of m and ε on location of neutral points

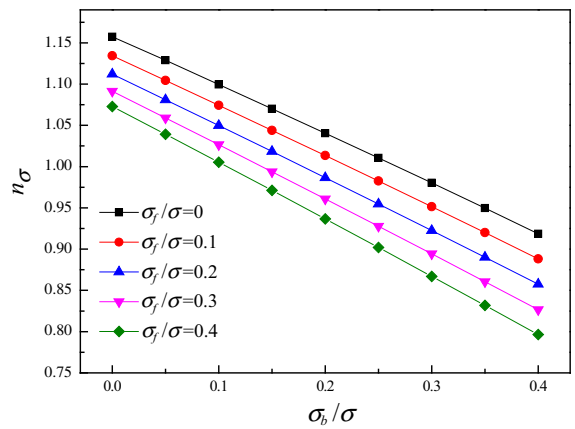

Fig. 8 Effect of tension stresses on n_σ

4.3 Influence of rolling parameters on stress state coefficient

In Fig. 8, the stress state coefficient $n_\sigma = F/(4blk)$ is a function of the backward and forward tension stresses. As the peak value of compression stress between roll-strip decreases when backward stress or forward tension stress increases, n_σ decreases linearly as σ_b or σ_f increases, especially for backward stress.

Figure 9 illustrates that the stress state coefficient n_σ has a positive correlation with friction factor m or reduction ε. In addition, the effect of reduction on the n_σ is marked.

5 Conclusions

The tangential velocity field and corresponding strain rate field are firstly proposed to be applied in tandem

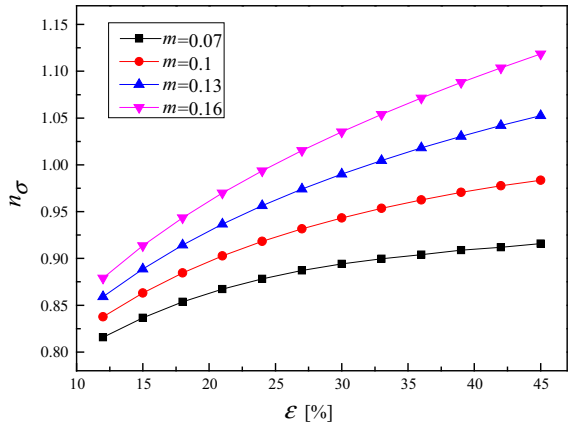

Fig. 9 Effect of ε and m on n_σ

cold rolling considering the effect of roll flattening on the roll separating force. The analytical solutions of roll separating force and stress effective factor are obtained based on elastic–plastic mechanics using energy method. The error of predicted roll-separating forces by present model is within +3.96% compared with measured ones in the plant and less than ±7.43% compared with Hill's results. The analytical solutions are reliable and adequate to research tandem cold rolling process. The neutral point moves toward the exit side while reduction and backward tension stress increase, or friction factor and forward tension stress decrease. The stress factor n_σ increases while reduction and friction factor increase, or forward tension stress and backward tension stress decrease.

Acknowledgements This study is financially supported by the National Natural Science Foundation of China (No.: 51074052, 50734002), the Fundamental Research Funds for the Central Universities (No.: N140704001), and National Intelligent Manufacturing Equipment Development Project of China (No.: 20142558).

Appendix 1

According to the concrete co-line vector inner product, the friction power $\dot{W}_f$ is

$$\begin{aligned}\dot{W}_f &= 4\int_0^l\int_0^b \tau_f|\Delta v_f|\mathrm{d}F = 4\int_0^l\int_0^b \boldsymbol{\tau}_f\Delta\boldsymbol{v}_f\mathrm{d}F\\ &= 4\int_0^l\int_0^b (\tau_{fx}\Delta v_x+\tau_{fy}\Delta v_y+\tau_{fz}\Delta v_z)\mathrm{d}F\\ &= 4mk\int_0^l\int_0^b (\Delta v_x\cos\alpha+\Delta v_y\cos\beta+\Delta v_z\cos\gamma)\mathrm{d}F\end{aligned} \tag{29}$$

where α, β, γ are the angles between $\boldsymbol{\tau}_f$ and the directions of x, y and z axes.

Since the tangential velocity discontinuity $\Delta\boldsymbol{v}_f$ and the tangent of the roll surface have the same direction, then the values of direction cosines can be determined by Eq. (1), and they are

$$\begin{aligned}\cos\alpha &= \pm\frac{\sqrt{R^2-(l-x)^2}}{R},\\ \cos\gamma &= \pm\frac{(l-x)}{R} = \sin\alpha,\quad \cos\beta = 0\end{aligned} \tag{30}$$

The differential element of the roll surface from Eq. (2) is

$$\mathrm{d}F = \sqrt{1+(h_x')^2}\mathrm{d}x\mathrm{d}y = \sec\alpha\mathrm{d}x\mathrm{d}y \tag{31}$$

The components of tangential velocity discontinuity $\Delta\boldsymbol{v}_f$ on roll surface from Eq. (3) are respectively:

$$\begin{aligned}\Delta v_x &= v_R\cos\alpha - v_0\left[1+\frac{1}{\lambda}\tan\left(\lambda\frac{h_0-h_x}{h_0}\right)\right]\\ \Delta v_y &= -v_0h_x'\left\{\frac{1}{h_0}\sec^2\left(\lambda\frac{h_0-h_x}{h_0}\right)\right.\\ &\quad\left.-\frac{1}{h_x}\left[1+\frac{1}{\lambda}\tan\left(\lambda\frac{h_0-h_x}{h_0}\right)\right]\right\}y\\ \Delta v_z|_{z=h_x} &= v_R\sin\alpha - v_0\tan\alpha\left[1+\frac{1}{\lambda}\tan\left(\lambda\frac{h_0-h_x}{h_0}\right)\right]\end{aligned} \tag{32}$$

Substituting Eqs. (30), (31) and (32) into Eq. (29) and integrating, then obtains

$$\begin{aligned}\dot{W}_f &= 4mkb\left\langle\int_0^l\left\{v_R\cos\alpha - v_0\left[1+\frac{1}{\lambda}\tan\left(\lambda\frac{h_0-h_x}{h_0}\right)\right]\right\}\mathrm{d}x\right.\\ &\quad\left.+\int_0^l\left\{v_R\sin\alpha - v_0\tan\alpha\left[1+\frac{1}{\lambda}\tan\left(\lambda\frac{h_0-h_x}{h_0}\right)\right]\right\}\tan\alpha\mathrm{d}x\right\rangle\\ &= 4mkb(I_1+I_2)\end{aligned} \tag{33}$$

$$\begin{aligned}I_1 &= \int_0^l\left\{v_R\cos\alpha - v_0\left[1+\frac{1}{\lambda}\tan\left(\lambda\frac{h_0-h_x}{h_0}\right)\right]\right\}\mathrm{d}x\\ &= \int_0^{x_n}\left\{v_R\cos\alpha - v_0\left[1+\frac{1}{\lambda}\tan\left(\lambda\frac{h_0-h_x}{h_0}\right)\right]\right\}\mathrm{d}x\\ &\quad-\int_{x_n}^l\left\{v_R\cos\alpha - v_0\left[1+\frac{1}{\lambda}\tan\left(\lambda\frac{h_0-h_x}{h_0}\right)\right]\right\}\mathrm{d}x\\ &= v_RR\left(\frac{\theta}{2}-\alpha_n+\frac{\sin 2\theta}{4}-\frac{\sin 2\alpha_n}{2}\right)\\ &\quad+\left(1+\frac{g_b}{\lambda}\right)v_0R(\sin\alpha_n-\sin\theta)+\left(1+\frac{g_f}{\lambda}\right)v_0R\sin\alpha_n\end{aligned} \tag{34}$$

Table 2 The measured data of deformation resistance

ε (%)	0.00	11.33	22.13	29.12	40.57	48.66	60.56	70.97	79.88	88.85
σ (MPa)	357.96	429.25	469.31	484.99	525.40	536.63	603.94	662.46	673.00	763.91

similarly

$$\begin{aligned} I_2 &= \int_0^l \left\{ v_R \sin\alpha - v_0 \tan\alpha \left[1 + \frac{1}{\lambda} \tan\left(\lambda \frac{h_0 - h_x}{h_0} \right) \right] \right\} \tan\alpha \mathrm{d}x \\ &= v_R R \left(\frac{\theta}{2} - \alpha_n + \frac{\sin 2\alpha_n}{2} - \frac{\sin 2\theta}{4} \right) \\ &\quad + \left(1 + \frac{g_b}{\lambda} \right) v_0 R \left[\ln \frac{(1+\cos\alpha_n + \sin\alpha_n)(1+\cos\theta - \sin\theta)}{(1+\cos\alpha_n - \sin\alpha_n)(1+\cos\theta + \sin\theta)} \right. \\ &\quad \left. + \sin\theta - \sin\alpha_n \right] \quad + \left(1 + \frac{g_f}{\lambda} \right) v_0 R \left(\ln \frac{1+\cos\alpha_n + \sin\alpha_n}{1+\cos\alpha_n - \sin\alpha_n} - \sin\alpha_n \right) \end{aligned} \tag{35}$$

Substituting Eqs. (34) and (35) into Eq. (33), and then Eq. (8) is gave.

Appendix 2

The form of MRT-2.5 steel deformation resistance model is chosen in this study as $\sigma = \left[A + \frac{B}{\sqrt{3}} \ln\left(\frac{H_0}{h}\right) \right] \left\{ 1 - C \cdot \exp\left[-\frac{D}{\sqrt{3}} \cdot \ln\left(\frac{H_0}{h}\right) \right] \right\}$. Taking some uniform initial thickness H_0 of strips, the measured deformation resistance values of MRT-2.5 steel after different rolling deformations are obtained as shown in Table 2. *A, B, C, D* are determined base on these experimental data.

And then the deformation resistance model in different reductions is obtained. So substituting $h = h_0$ into deformation resistance model obtains the deformation resistances at entry side σ_{sin} in Eq. (26); substituting $h = h_1$ into deformation resistance model obtains the deformation resistances at exit side σ_{sout} in Eq. (27).

References

1. Tselikov AI (1958) Present state of theory of metal pressure upon rolls in longitudinal rolling. Stahl 18(5):434–441
2. Bland DR, Ford H (1948) The calculation of roll force and torque in cold strip rolling with tensions. Proc Inst Mech Eng 159(1):144–163. doi:10.1243/pime_proc_1948_159_015_02
3. Orowan E (1943) The calculation of roll pressure in hot and cold flat rolling. Proc Inst Mech Eng 150(1943):140–167. doi:10.1243/pime_proc_1943_150_025_02
4. Hill R (1950) Relations between roll-force, torque, and the applied tensions in strip-rolling. Proc Inst Mech Eng 163(1):135–140. doi:10.1243/pime_proc_1950_163_017_02
5. Stone MD (1953) Rolling of thin strip. Iron Steel Eng 30(2):1–15
6. Freshwater IJ (1996) Simplified theories of flat rolling-I. The calculation of roll pressure, roll force and roll torque. Int J Mech Sci 38(6):633–648. doi:10.1016/0020-7403(95)00072-0
7. Freshwater IJ (1996) Simplified theories of flat rolling-II. Comparison of calculated and experimental results. Int J Mech Sci 38(6):649–660. doi:10.1016/0020-7403(95)00739-3
8. Hu PH, Ehmann KF (2000) A dynamic model of the rolling process. Part I: homogeneous model. Int J Mach Tools Manuf 40(1):1–19. doi:10.1016/S0890-6955(99)00049-8
9. Hu PH, Ehmann KF (2000) A dynamic model of the rolling process. Part II: inhomogeneous model. Int J Mach Tools Manuf 40(1):21–31. doi:10.1016/S0890-6955(99)00050-4
10. Le HR, Sutcliffe MPF (2001) A robust model for rolling of thin strip and foil. Int J Mech Sci 43(6):1405–1419
11. Chen SZ, Zhang DH, Sun J, Wang JS, Song J (2012) Online calculation model of rolling force for cold rolling mill based on numerical integration. In: Chinese control and decision conference, pp 3951–3955
12. Guo RM (2010) New approaches to roll bite behaviors with multiple characteristic zones. In: Proceedings of the 10th international conference on steel rolling, pp 1605–1612
13. Guo RM (2014) Investigation of roll bite behavior with various cold rolling conditions using semi-analytic solutions of Von Karman's rolling equation. Metall Ital 4:29–38
14. Zhao DW (2002) Material forming mechanics. Northeastern University Press, Shenyang
15. Sezek S, Aksakal B, Can Y (2008) Analysis of cold and hot plate rolling using dual stream functions. Mater Des 29(3):584–596. doi:10.1016/j.matdes.2007.03.005
16. Malinowski Z, Pietrzyk M, Lenard J (1993) Analysis of the flat-rolling process: one-dimensional and finite-element models. J Mater Process Technol 39(3):373–387
17. Lin ZC, Lin VH (1995) Analysis of the variation of the cold-rolling characteristics of rolling force, strip shape, stress and temperature, for a three-dimensional strip. J Mater Process Technol 54(1):326–340. doi:10.1016/0924-0136(95)01796-8
18. Reddy NV, Suryanarayana G (2001) A set-up model for tandem cold rolling mills. J Mater Process Technol 116(2):269–277
19. Jiang ZY, Tieu AK, Zhang XM, Lu C, Sun WH (2003) Finite element simulation of cold rolling of thin strip. J Mater Process Technol 140(1):542–547. doi:10.1016/S0924-0136(03)00832-X
20. Montmitonnet P (2006) Hot and cold strip rolling processes. Comput Methods Appl Mech Eng 195(48):6604–6625. doi:10.1016/j.cma.2005.10.014
21. Zhang SH, Song BN, Wang XN, Zhao DW, Chen XD (2014) Deduction of geometrical approximation yield

criterion and its application. J Mech Sci Technol 28(6):2263–2271. doi:10.1007/s12206-014-0515-6
22. Liu YM, Ma GS, Zhang DH, Zhao DW (2015) Upper bound analysis of rolling force and dog-bone shape via sine function model in vertical rolling. J Mater Process Technol 223:91–97. doi:10.1016/j.jmatprotec.2015.03.051
23. Jiang ZY, Tieu AK, Lu C (2004) A FEM modelling of the elastic deformation zones in flat rolling. J Mater Process Technol 146(2):167–174. doi:10.1016/j.matprotec.2003.10.012
24. Ginzburg VB, Ballas R (2000) Flat rolling fundamentals. Marcel Dekker, New York